Ecdysone-mediated intestinal growth contributes to microbiota-driven developmental plasticity under malnutrition

Longwei Bai[1], Stéphanie Bellemin[1,2], Elodie Guillemot[1,3], Maura Strigini[1,4], Benjamin Gillet[1], Cathy Isaura Ramos[1]*, François Leulier[1*%]

[1] Institut de Génomique Fonctionnelle de Lyon, Ecole Normale Supérieur de Lyon, CNRS UMR 5242, Université Claude Bernard Lyon 1, 46 allée d'Italie, 69007 Lyon, France

[2] Present address : Synbird, 14 Fbg Reclus, 73000 Chambéry, France
[3] Present address : Charles River Laboratories, 9 All. Moulin Berger, 69130 Écully, France
[4] Present address : Université Jean Monnet Saint-Étienne, Mines Saint Etienne, INSERM, SAINBIOSE U1059, 42023 Saint-etienne, France

*Co-senior authors
[%] Correspondance: francois.leulier@ens-lyon.fr

Acknowledgements
The authors would like to thank Berra Erkosar for initial observations; Coralie Drelon for experimental support and Pauline Joncour for bioinformatic support; Naoki Yamanaka for sharing reagents at the early stage of the project; Aurelio Teleman and Gilles Storelli for discussions; the IGFL sequencing and imaging facilities; the PLATIM and Arthro-Tools platforms at the SFR Biosciences Lyon Gerland (UAR3444/US8) for providing Imaging and *Drosophila* facilities; the Bloomington Drosophila Stock Center (BDSC) and Vienna Drosophila Ressource Center (VDRC) for fly stocks and Developmental Studies Hybridoma Bank (DSHB) for antibodies**.**

Competing interests
The authors declare no competing or financial interests.

Author contributions
Conceptualization: F.L. and C.I.R.; Methodology: F.L., C.I.R., L.B., S.B. and M.S.; Validation: F.L., C.I.R., L.B. and S.B.; Formal analysis: L.B., C.I.R.; Investigation: L.B., E.G., B.G. and C.I.R.; Resources: C.I.R., L.B., and B.G.; Data curation: L.B. and C.I.R.; Writing - original draft: L.B., C.I.R. and F.L.; Writing - review & editing: L.B., C.I.R. and F.L.; Visualization: L.B. and C.I.R; Supervision: F.L. and C.I.R.; Project administration: C.I.R and F.L..; Funding acquisition: F.L. and C.I.R.

Funding
This project was supported by the "Fondation pour la Recherche Médicale" (Equipe FRM DEQ20180339196 – to F.L.), the Scientific Breakthrough Project from Université de Lyon (Project "Microbehave" - to F.L.), an ERC starting grant (FP7/2007-2013-N°309704 - to F.L.), UCBL BQR (to C.I.R.) and FINOVI AO12-19-Projet SNI (to C.I.R.). L.B. was funded by a Chinese Government Scholarship.

Keywords
Adaptive growth, developmental plasticity, ecdysone signaling, microbiota, intestine, *Drosophila*.

Abstract

Organ and systemic growth must remain coordinated during development, even under nutritional stress. In *Drosophila* larvae, the intestinal microbiota contributes to this coordination by promoting growth and maturation under chronic undernutrition. Using gnotobiotic models, we show that association with *Lactiplantibacillus plantarum* (*Lp*) selectively enhances midgut growth relatively to other organs, providing an adaptive mechanism that buffers the impact of dietary restriction. Transcriptomic profiling of larval midguts revealed a strong Ecdysone signaling signature upon *Lp* association. Functional analyses showed that local conversion of Ecdysone to its active form, 20-hydroxyecdysone, by the cytochrome P450 enzyme Shade, together with enterocyte Ecd receptor activity, is required for *Lp*-dependent intestinal and systemic growth. Pharmacological activation of Ecd signaling partially mimicked the bacterial effect, confirming its sufficiency to drive adaptive midgut expansion. Our results uncover an unexpected role of intestinal Ecd signaling in microbiota-driven developmental plasticity, revealing how commensal bacteria modulate local steroid signaling to fine-tune organismal growth and maturation.

Introduction

In animals, organ growth is coordinated with systemic growth to ensure synchronized development. Beyond this coordination, organisms exhibit developmental plasticity, the ability to adjust growth and maturation rates in response to environmental and internal cues, ensuring the emergence of fit adults (Pigliucci, 2001). Nutrition is a major regulator of developmental plasticity, and the microbiota has emerged as another key determinant of this process (Storelli et al., 2011, Shin et al., 2011).

In *Drosophila* larvae, nutrient restriction delays growth and development. The absence of a microbiota further exacerbates this delay, whereas mono-association of germ-free (GF) animals with *Lactiplantibacillus plantarum* (*Lp*), a representative member of the fly microbiota, restores both growth and maturation rates (Storelli et al., 2011). These beneficial effects of *Lp* depend on enhanced digestive capacity and improved systemic growth signaling under chronic undernutrition (Erkosar et al., 2015, Matos et al., 2017, Storelli et al., 2018).

Adaptive developmental responses in *Drosophila* are primarily governed by two hormonal systems: Insulin-like peptides (Ilps), which control systemic growth rate (Colombani et al., 2003, Geminard et al., 2009), and the steroid hormone ecdysone (Ecd), which determines the duration of growth periods by triggering molting and maturation (Shingleton et al., 2005). Microbiota-dependent developmental acceleration involves both axes through TORC1 activation in the fat body and prothoracic gland (PG) (Storelli et al., 2011).

Ecd is synthesized from dietary cholesterol in the PG under control of the prothoracicotropic hormone, secreted into the hemolymph, and taken up by peripheral tissues through Organic Anion Transporting Polypeptides such as the Ecdysone Importer EcI/Oatp74D (Okamoto et al., 2018, Okamoto and Yamanaka, 2020). Once internalized, Ecd is converted by the cytochrome P450 enzyme Shade into its active form, 20-hydroxyecdysone (20E), which binds to the Ecdysone receptor (EcR) to regulate gene expression (Petryk et al., 2003, Yamanaka et al., 2015).

While the systemic and local actions of Ilps are well understood, the tissue-specific contributions of Ecd remain poorly characterized, owing to its pleiotropic effects on growth, remodeling, and differentiation across larval and imaginal tissues (Boulan et al., 2015). How these canonical systemic signals translate into tissue-specific growth responses during nutritional stress remains largely unknown. Here, we identify intestinal Ecd signaling as a key mediator of microbiota-dependent developmental plasticity. Transcriptomic and functional analyses reveal that *Lp* association enhances Ecd signaling in larval enterocytes during malnutrition, promoting adaptive intestinal growth that contributes to systemic developmental coordination.

Results and Discussion

95

Microbiota association selectively promotes midgut growth under malnutrition

To assess how *Lp* influences organ growth during chronic malnutrition, we compared the growth of diploid (central nervous system, wing discs) and polyploid (salivary glands, midgut) larval organs in GF and *Lp*-associated conditions (Fig. 1A). While the CNS, wing discs, and salivary glands were
100 comparable between GF and *Lp*-associated larvae (Fig. 1B–D), the midgut displayed a robust increase in length (Fig. 1E–F). Thus, the larval midgut is a primary target of microbiota-mediated growth under nutrient restriction.

To determine whether this growth occurred uniformly along the gut, we examined anterior, middle, and posterior regions separately. Despite *Lp* colonizing mainly the anterior half of the midgut (Storelli
105 et al., 2018), both anterior and posterior regions were significantly longer in *Lp*-associated larvae (Fig. 1G–L). Increased enterocyte size in these regions (Fig. 1M–N; Fig. S1) indicates that *Lp*-mediated midgut growth results at least in part from enhanced cell growth.

These findings demonstrate that *Lp* association triggers a coordinated growth response within the larval midgut. The spatial distribution of this effect, which does not mirror bacterial abundance,
110 suggests that *Lp*-induced signals may propagate along the gut or act through systemic factors. Recent work in the adult intestine (Blackie et al., 2024) highlights functional coupling between distinct epithelial compartments through spatial proximity and signaling cross-talk, raising the possibility that folded larval midgut regions also interact dynamically within the larval milieu. Furthermore, the observation that both anterior and posterior but not the middle segment enlarge upon *Lp*
115 association suggests potential functional heterogeneity among intestinal cell populations, possibly linked to differential hormonal responsiveness.

Microbiota association induces an intestinal ecdysone signaling signature

To uncover transcriptional programs underlying microbiota-dependent intestinal growth, we performed RNA sequencing on midguts dissected from size-matched GF and *Lp*-associated larvae at
120 early and late third-instar (L3) stages (Fig. 2A, Fig. S2A–B). This design controlled for *Lp*-induced developmental acceleration. Transcriptomic profiling identified 2,633 differentially expressed genes across both stages. Functional clustering (DAVID) yielded 91 annotation clusters, with the strongest enrichment for “Ecdysteroid kinase-like” genes, followed by categories related to mitochondrial activity, proteolysis, and signal transduction (Fig. S2C–D). Gene Ontology analysis revealed a unique
125 enrichment for the “Response to ecdysone” term (Fig. S3), and several canonical ecdysone-responsive genes were upregulated in *Lp*-associated midguts (Fig. S4A).

Differential expression was extensive at both stages (early L3: 1,624 genes; late L3: 1,462 genes), with a predominance of upregulated transcripts (Fig. 2B). As expected, *Lp* association induced IMD pathway targets (*PGRP-SC1*, *PGRP-SC2*, *Pirk*) and markers of intestinal maturation (*jon66cii*, *jon44E*;
130 Fig. S5A–B). In contrast, canonical growth regulators (*Dilps*, *dMyc*, *Hippo*, *EGFR*) were unchanged (Fig. S4B), indicating that microbiota-driven midgut growth operates through alternative mechanisms. RT-qPCR confirmed the RNA-seq results, showing increased expression of EcR target genes in midguts

from *Lp*-associated larvae but not from animals colonized with heat-killed bacteria (Fig. 2C–E). These findings demonstrate that live *Lp* bacteria are required to induce intestinal Ecd signaling under malnutrition. Altogether, these data reveal that *Lp* association activates a distinct intestinal ecdysone signaling program, identifying Ecd as a candidate hormonal mediator of microbiota-driven adaptive growth.

Enterocyte ecdysone signaling mediates microbiota-dependent intestinal growth

Because *Lp* promotes systemic growth and induces intestinal Ecd targets, we next examined whether Ecd signaling is required for midgut adaptation. Quantification of 20E showed significant elevated levels in both midgut and hemolymph of size-matched *Lp*-associated larvae compared with GF controls, whereas fat body levels were slightly elevated (Fig. 3A–C).

Reducing *EcR* expression specifically in enterocytes by RNAi markedly suppressed *Lp*-dependent midgut growth and gut-to-carcass ratios (Fig. 3D–E; Fig. S5C), demonstrating that enterocyte EcR activity is necessary for the bacterial effect. Similarly, silencing *shade* also reduced *Lp*-dependent growth (Fig. 3F–G; Fig. S5D). Because Shade is enriched in the larval midgut (Chung et al., 2009, Brown et al., 2014), these results indicate that *Lp* enhances local Ecd activation in enterocytes.

Finally, dietary supplementation with the nonsteroidal Ecd agonist RH5849 (Wing, 1988) modestly increased midgut length in GF larvae without affecting developmental timing (Fig. 3H–J), indicating that activation of intestinal Ecd signaling is sufficient to partially reproduce the *Lp*-induced intestinal growth effect.

Intestinal ecdysone signaling supports systemic growth adaptation during microbiota association

To test whether intestinal Ecd signaling also contributes to systemic developmental outcomes, we silenced *EcR* or *shade* in specific tissues and measured developmental timing and pupal size during malnutrition (Fig. 4; Fig. S6A–D). Disrupting Ecd signaling in the fat body using *Lpp*-GAL4 slightly delayed development in both GF and *Lp*-associated larvae and triggered full pupal lethality in all conditions, stressing the essential role of fat-body Ecd responses for proper developmental progression and metamorphosis. In contrast, enterocyte-specific *EcR* knockdown delayed pupariation only in GF animals (Fig. 4A,C), while *Lp*-associated counterparts developed as controls. *shade* knockdown did not affect timing in either condition (Fig. 4B,D). Notably, both *EcR*- and *shade*-RNAi *Lp*-associated larvae produced significantly smaller pupae than controls (Fig. 4E–F).

These findings indicate that while fat-body Ecd signaling regulates developmental tempo and ensures developmental transitions such as metamorphosis, intestinal Ecd activity specifically supports systemic growth adaptation during *Lp* association. Thus, microbiota-enhanced enterocyte Ecd signaling contributes to both local gut expansion and organismal growth plasticity under nutrient restriction.

Conclusion

Together, our findings reveal that organ and systemic growth remain tightly coordinated even under nutritional stress, and that this coordination relies on microbiota-mediated modulation of intestinal

physiology. Under malnutrition, association with *Lactiplantibacillus plantarum* promotes enterocyte growth and intestinal expansion, providing an adaptive mechanism that buffers the impact of dietary restriction on developmental growth.

Transcriptomic and functional analyses identify intestinal Ecd signaling as a key mediator of this adaptive response. *Lp* association enhances the local conversion of Ecd to its active form 20E, through Shade activity, and both Shade and the EcR are required for *Lp*-dependent intestinal and systemic growth. These results establish intestinal Ecd signaling as a central hormonal component of microbiota-driven developmental plasticity.

Recent studies have emphasized that Ecdysone signaling in adult enterocytes orchestrates cellular hypertrophy and endoreplication to control midgut size and functionality (Ahmed et al., 2020, Zipper et al., 2025, Zipper et al., 2020). Integrating these findings with our work suggests that the microbiota leverages this local Ecdysone-dependent growth program to tune intestinal capacity according to nutritional availability in the context of larval development. This highlights Ecdysone signaling in enterocytes as a pivotal interface between microbial cues, tissue plasticity, and systemic developmental control and calls for investigating the contribution of microbiota to adult intestinal plasticity.

By uncovering a direct link between commensal bacteria, intestinal steroid signaling, and systemic growth control, this work expands the physiological framework of Ecd action beyond its classical endocrine role. It highlights how local steroid signaling within an epithelial organ can exert systemic influence on growth, revealing a new level of developmental coordination between tissues and their microbial partners. Similar microbiota–steroid interactions occur in mammals, where gut bacteria, including *Lactobacillus* species, produce β-glucuronidase enzymes that reactivate estrogens (Baker et al., 2017, Ervin et al., 2019, Hu et al., 2023). Given the functional analogies between Drosophila Ecdysone and mammalian estrogens (Aranda and Pascual, 2001, Martinez et al., 1991, Oberdorster et al., 2001), our findings suggest that microbiota-mediated modulation of steroid activity represents an evolutionarily conserved mechanism linking microbial cues to host endocrine control. It positions the larval midgut as an adaptive interface integrating nutritional, microbial, and hormonal cues to fine-tune organismal maturation.

200 **Methods**

Fly stocks and media

Conventional *Drosophila* stocks were reared at 25°C under a 12:12 hour light/dark cycle using a standard cornmeal-yeast medium containing 8.2 g/L agar (#20768.361, VWR), 80 g/L cornmeal flour
205 (Westhove, Farigel maize H1), 80 g/L inactivated yeast (#24979.413, VWR), and supplemented with 5.2 g/L Methyl 4-hydroxybenzoate sodium salt (#106756, Merck) and 4 mL/L of propionic acid (#409553, Carlo Elba). The axenic embryos were generated as previously described (Ma et al., 2015). These sterilized embryos were subsequently raised on a standard medium that included a cocktail of four antibiotics (Ampicillin, Kanamycin, Tetracycline, and Erythromycin) to maintain a GF
210 environment for the newly hatched larvae. The nutritional challenge was performed using fresh food where the amount of inactivated yeast was reduced to 7 g/L (referred as to low-yeast diet). The following fly stocks were used: *yw* (obtained from Bruno Lemaitre), *mex-GAL4* (obtained from Irene Miguel-Aliaga), *Lpp-GAL4* (obtained from Alexandre Djiane), *UAS-EcR* RNAi (BDSC#9327), *UAS-shade* RNAi (VDRC#108911), and respective TRiP control line (BDSC# 35785) and KK control line
215 (VDRC#60101). All experimental crosses were performed at 29°C and females laid eggs on low-yeast food.

Bacterial culture and larvae mono-association

Lp^{WJL} referred to *Lp* in this manuscript (Storelli et al., 2011) was cultured overnight in Man, Rogosa
220 and Sharpe (MRS) broth at 37°C without shaking. For inoculation, tubes containing 40–60 GF embryos were seeded with resupened *Lp* to achieve a final dose of 10^8 CFUs/tube. As a control, bacteria were inactivated by heat using a 95°C water bath treatment for 45 min. For GF controls, an equal volume of sterile PBS was applied.

225 **RNA sequencing**

GF or *Lp*-associated *yw* axenic embryos were reared on a low-yeast diet. Gut collection from L3 larvae was performed to obtain size-matched larvae: early L3 samples (15 guts/replicate, 5 replicates) were collected at 4 days AEL for *Lp* and 8 days AEL for GF, while late L3 samples (10 guts/replicate, 5 replicates) were collected at 6 days AEL for *Lp* and 10 days AEL for GF. RNA was
230 extracted using the NucleoSpin kit (Macherey Nagel, #740955) following the manufacturer's protocol, and quantified using the Nanodrop spectrophotometer (Thermofisher, ND-2000).
For RNA sequencing, samples were treated by the IGFL sequencing platform. Purification, quantification and quality checks were performed using the Qubit 2.0 – RNA BR Assay Kit (Thermofisher) and the TypeStation 2200 (Agilent). Libraries were generated following the online
235 protocol (https://www.hexabiogen.com), quantified via the TapeSation D1000 ScreenTape Assay (Agilent), and the raw data were subsequently processed to generate final genes regulation datasets as in (Grenier et al., 2023). The sequencing data were analyzed using the DAVID Bioinformatics Resources online software (https://david.ncifcrf.gov/) on 2633 annotated genes across both sizes groups, which were organized into a functional annotation chart and subsequently grouped into 91
240 clusters. An enrichment score (ES) was calculated (ES = $-\log_{10}$ mean of the adjusted *P* value (P_{adj})) and 53 of the clusters were found to be significantly enriched (ES >1.3, corresponding to $P_{adj} < 0.05$). Then, genes from the two sizes were split into early L3 and late L3 groups and further analyzed by

Biological Process Direct with $P_{adj} < 5.1\times 10^{-2}$ and presented as pie charts. Finally, volcano plots were generated using GraphPad Prism 10.

245

RT-qPCR

RNA was extracted from ten dissected guts of size-matched larvae after homogenization with glass beads in a Precellys 24 and purified using the NucleoSpin kit (Macherey-Nagel). Reverse transcription of 1µg of RNA was performed with SuperScript II (Invitrogen). Quantitative PCR (qPCR) was run on an
250 iQ5 Real-time PCR Detection System (Biorad) using SYBR GreenER qPCR SuperMix (Invitrogen). Specific and unique amplification was confirmed by melting curve analysis. All expression levels were normalized to two reference genes, *Tubulin* and *RpL32* using delta-delta-Ct method. The following primers (5'–3') were used for qPCR assays: *tubulin* qF TGTCGCGTGTGAAACACTTC, qR AGCAGGCGTTTCCAATCTG; *RpL32* qF ATGCTAAGCTGTCGCACAAATG, qR
255 GTTCGATCCGTAACCGATGT; *jon66Cii* qF AAACTGACCCCGGTCCAC, qR CCTCCTCAGCCGGATAGC; *EcR* qF GCAAGGGGTTCTTTCGACG, qR CGGCCAGGCACTTTTTCAG; *jon44E* qF ACAGCGCTAACCATGTGCT, qR GGTGTACTGGGCCTCGTG; *shade* qF CCCACCAAAACGTACAGGGA, qR GTAATCCAGCAGCCTCGTCA; *Eip74EF* qF CATAAAGACGGAGCAAAATACGC, qR CCGCTAAGCAGATTGTGGAG; *Eip75B* qF ATCTGCATGTTTGACTCGTCG, qR
260 TCCGCGAAATTGAAGGTGGAG.

Developmental timing determination and pupal volume analysis

40 or 60 (in RNAi conditions) axenic eggs were inoculated with *Lp* or sterile PBS (control) and incubated at 25°C (experiments using *yw* animals) or 29°C (RNAi experiments). Larval developmental
265 timing was assesses by daily counting the number of new-emerged pupae until all pupae emerged. Median time to pupariation was calculated to evaluate larval developmental timing. Pupae were imaged using a stereomicroscope (M205FA, Leica). Measurements for length (L) and width (W) were taken using Fiji software (Version 1.54r), and the pupal volume was calculated using the formula $(4/3)\ \pi(L/2)\ (W/2)^2$.

270

Measurement of 20E titers

Ten guts or five fat bodies were dissected from *yw* L3 larvae and pooled in 200 µL of MeOH. Samples were ground with a pestle and vortexed. After adding 300 µL of MeOH, samples were centrifuged for 10 min, 13,000g at 4˚C. The supernatant was kept in a new tube and the pellet was re-extracted with
275 500 µL MeOH, vortexed and centrifuged. Finally, the last extraction was performed using 500 µL EtOH. The three collected supernatants were pooled and stored at -20˚C. For normalization, a duplicate of this experiment was performed and samples were quantify using BCA assay kit (SIGMA). For haemolymph, *yw* L3 larvae were dried on tissue paper and placed on parafilm. The cuticle was gently pricked to collect 2 µL haemolymph from 8 larvae that were placed in 200 µL of MeOH. Then,
280 the samples were treated the same way as described above. Most extraction steps were performed on ice. Evaporation of the samples was done using a SpeedVac and then dissolved in EIA buffer from the kit (A05120, Bertin) and treated following the manufacturer's instructions.

Nonsteroidal Ecd agonist treatments

285 *yw* axenic embryos were transferred to freshly prepared low-yeast fly medium, which was supplemented with the nonsteroidal Ecd agonist RH5849 (5 µg/mL) (DRE-C16813000,

DrEhrenstorfer) or an equal volume of MeOH as a vehicle control. The flies were then reared at 25°C for the subsequent developmental timing and gut size measurements.

Organ morphometric analysis

Lp-associated larvae (5–7 days AEL) and GF larvae (8–11 days AEL) were collected during the middle to late L3 instar (pre-wandering). Four organs were dissected from each larva, directly oriented on a poly-Lysine coated slide, and imaged using a stereomicroscope (M205FA, Leica). Organ area/length was measured. Data were analyzed using log-log plots to determine the allometric scaling relationship $y = bx^{\alpha}$ (Huxley, 1924).

Gut morphometry and cell area analysis

L3 instar larval guts were dissected, immediately fixed for 1 min in Bouin's solution (HT10132, Sigma) and kept attached to the corresponding carcass for body length determination. Guts were imaged using a stereomicroscope (M205FA, Leica). Gut length was measured and normalized as the gut length/carcass length ratio to account for size variability between larvae.

For cell area analysis, L3 larval guts were dissected and fixed in Bouin's solution for 2 min and washed in PBST (PBS with 0.5% Triton X-100). After saturation with Normal Goat Serum (G9023, Sigma), mouse anti-Dlg primary antibody (4F3, DSHB) was incubated, at a 1:1000 dilution overnight at 4˚C. After washes, Alexa Fluor 555 anti-mouse conjugated secondary antibodies (Molecular Probes) were added at 1:200 for 2 h at room temperature. After final washes, samples were mounted in Vectashield Mounting Medium with DAPI (H-1800, Vector Laboratories) and images were acquired as mosaics using the DM6000 (Leica) and analyzed with the Fiji software (Version 1.54r).

Statistical analysis

Statistical analysis and data visualization were performed using GraphPad Prism 10 software (version 10.6.1). The number of biological replicates (*n*), specific statistical tests, and error bar definitions are detailed in the corresponding figure legends. *P* values are indicated directly on the figures.

Graphics

Schematics were created with BioRender.

Declaration of generative AI and AI-assisted technologies in the writing process

During the preparation of this work, the authors used ChatGPT.5 in order to polish the language of the manuscript. After using this tool, the authors reviewed and edited the content as needed and take full responsibility for the content of the publication.

Figures legends

Figure 1. Microbiota association selectively promotes midgut growth under malnutrition

(A) Experimental roadmap detailing organ collection for L3 instar *yw* larvae: Lp^{WJL}-associated (D5–D7) and GF (D8–D11). *n* = number of dissected larvae.

(B–E) Allometric scaling of organ size/organ area vs. body length for: (B) CNS, (C) imaginal wing discs, (D) salivary glands, and (E) midguts. Simple linear regressions are shown for each group. *P* values for the allometric interaction (slope difference) and the Lp^{WJL} effect (elevation difference) are indicated.

(F) Representative images of dissected guts attached to their respective carcasses (body length readout, green line) from Lp^{WJL}-associated (D6) and GF larvae (D9). Red, orange, and yellow lines indicate the anterior, middle, and posterior gut regions, respectively. Scale bar represents 5 µm.

(G–L) Quantification of gut size in size-matched GF and Lp^{WJL}-associated larvae. (G) Larval size. (H) Whole gut length. (I–L) Normalized gut length (gut length/carcass length ratio) for the whole gut (I), anterior gut (J), middle gut (K), and posterior gut (L). *n* = 6.

(M–N) Quantification of enterocyte cell area in the anterior (M) and posterior (N) gut regions. *n* = 7.

In all panels, purple indicates Lp^{WJL}-associated larvae and GF larvae in gray. Statistical significance was determined using a two-tailed unpaired *t*-test (G–J, L, N) and a lognormal *t*-test (K, M). *P* values are indicated on the panels.

Figure 2. Microbiota association induces an intestinal ecdysone signaling signature

(A) Experimental roadmap detailing midgut collection from size-matched Lp^{WJL}-associated and GF larvae at two developmental stages: early L3 and late L3.

(B) Volcano plots illustrating differential gene expression between Lp^{WJL}-associated and GF midguts at early L3 (upper panel) and late L3 (bottom panel) instars. All genes are shown in the left panel, while the right panel highlights genes with a strong significance ($10 < -\log10 (P_{adj}) < 50$).

(C–E) Relative transcript levels of ecdysone-responsive genes in the gut—*EcR* (C), *Eip74EF* (D), and *Eip75B* (E) were analyzed by qRT-PCR in GF, Lp^{WJL}-associated, and heat-killed (HK) Lp^{WJL}-associated larvae under malnutrition. Data are presented as mean ± SEM. Statistical significance was determined using one-way ANOVA with Tukey's multiple comparisons test. *P* values are indicated on the panels. *n* = 5.

Figure 3. Enterocyte ecdysone signaling mediates microbiota-dependent intestinal growth

(A–C) Quantified 20E levels in the haemolymph (A), midgut (B), and fat body (C) of size-matched GF and Lp^{WJL}-associated larvae. *n* = 5.

(D–G) Measured gut length in size-matched GF and Lp^{WJL}-associated larvae with *EcR* knockdown in enterocytes (ECs) (*mex>EcR* RNAi) (D) and *shade* knockdown (*mex>shade* RNAi) (F). Normalized gut length with *EcR* RNAi (E) and *shade* RNAi (G) was also determined. Controls included respective TRiP and KK lines. *n* ≥ 10.

(H–J) Quantified median time to pupariation (H), gut length (I), and normalized gut length (J) in *yw* GF larvae fed the ecdysone agonist RH5849 compared to a MeOH vehicle control. *n* ≥ 7.

Statistical significance was determined using a two-tailed Welch's *t* test (A), a lognormal *t*-test (B–C), a two-way ANOVA with Tukey's multiple comparisons test (D–G), a two-tailed unpaired *t* test (H), and a two-tailed Mann-Whitney *U* test (I–J). *P* values are indicated on the panels.

Figure 4. Intestinal ecdysone signaling supports systemic growth adaptation during microbiota association

Under malnutrition, measured developmental timing (A–B), corresponding median time to pupariation (C–D), and pupal volumes (E–F) are shown in GF and Lp^{WJL}-associated larvae with *EcR* knockdown in ECs (*mex>EcR* RNAi) (A, C, E) and *shade* knockdown (*mex>shade* RNAi) (B, D, F). Controls included respective TRiP and KK lines. Statistical significance was determined using a two-way ANOVA with Tukey's multiple comparisons test. *P* values are indicated on the panels. (A–D): $n \geq 8$. (E–F): $n \geq 65$.

Supplementary Figures legends

380 **Figure S1 (related to Figure 1). *Lp^{WJL}* mediates midgut growth through cell area increase.**
Representative images of anterior and posterior midguts from size-matched *Lp^{WJL}*-associated (D7) and GF (D11) *yw* larvae. Midguts were dissected and stained for Discs large (Dlg, red), a septate junction marker, and DAPI (blue) to mark nuclei. Scale bar represents 100 µm.

385 **Figure S2 (related to Figure 2). Midgut transcriptomic analysis pinpointes *Lp^{WJL}*-triggered EcKL cluster.**
(A–B) Principal Component Analysis (PCA) plots in (A) show the samples grouped by size, distinguishing Size 1 (green) and Size 2 (blue), with the computed centers for GF and *Lp^{WJL}* samples indicated in purple, while the PCA in (B) plots samples based on microbial association, distinguishing *Lp^{WJL}*-associated (red)
390 and GF (black) samples, with the computed centers for Size 1 and Size 2 within the GF and *Lp^{WJL}* groups shown in purple.
(C–D) RNA sequencing results identified 2633 annotated genes that were differentially regulated by *Lp^{WJL}* in both sizes; a total of 53 gene clusters (out of 91) were found to be enriched with a score (ES) > 1.3 ($P < 0.05$) (C), and genes belonging to the "EcKL" (Ecdysteroid Kinase like) cluster showed the
395 highest enrichment score.

Figure S3 (related to Figure 2). Ecd-responsive biological processes in early L3 and late L3 undernourished larvae.
Biological Processes (BP Direct, $P_{adj} < 5.1\times 10^{-2}$) responsive to Ecd are summarized in pie charts for early
400 L3 and late L3 larvae. The pie charts feature boxes highlighting specific BPs: where those found only in early L3 are in normal font, those found only in late L3 are in bold, and those common to both stages are in bold with underlines.

Figure S4 (related to Figure 2). Ecd and tissue growth effector gene expression under *Lp^{WJL}*
405 **association.**
Panels (A) and (B) show gene expression data illustrating the differential effect of *Lp^{WJL}* association versus GF conditions in L3 larvae. Specifically, the Ecd related genes and the “EcKL” cluster genes were listed in (A), while canonical effectors involved in tissue growth are listed in (B). Mean read counts for both conditions ("Mean GF" and "Mean *Lp^{WJL}*") and the Fold Change (FC) are shown. The
410 mean of the reads counted are presented as “Mean GF” and “Mean *Lp^{WJL}*”. FC is indicated by a color code (red for upregulation, yellow for no change, and green for downregulation), with accompanying raw *P* values and adjusted *P* values (P_{adj}).

Figure S5 (related to Figure 3). Validation of intestinal peptidases gene expression and knockdown
415 **efficiency of Ecdysone effectors.**
(A–B) The transcript levels of intestinal peptidases *jon66Cii* (A) and *jon44E* (B) were analyzed by qRT-PCR in undernourished GF and *Lp^{WJL}*-associated *yw* larvae. n ≥ 5.
(C–D) The RNAi efficiency of *EcR* and *shade* in ECs was validated via qRT-PCR in undernourished GF larvae. n ≥ 3.
420 Data are shown as mean ± SEM. Statistical significance was determined using a two-tailed Welch’s *t* test (A, D), a two-tailed unpaired *t* test (B), and a two-tailed Mann-Whitney *U* test (C). *P* values are indicated on the panels.

Figure S6 (related to Figure 4). Knowdown of fat body-derived Ecd signaling causes mild developmental delay under malnutrition.

(A–D) Under malnutrition, measured developmental timing (A–B) and corresponding median time to pupariation (C–D) are presented in GF and Lp^{WJL}-associated larvae with *EcR* knockdown in the fat body (*Lpp>EcR* RNAi) (A, C) and *shade* knockdown (*Lpp>shade* RNAi) (B, D). Controls included respective TRiP and KK lines. Statistical significance was determined using a two-way ANOVA with Tukey's multiple comparisons test. *P* values are indicated on the panels. $n \geq 8$.

References

AHMED, S. M. H., MALDERA, J. A., KRUNIC, D., PAIVA-SILVA, G. O., PENALVA, C., TELEMAN, A. A. & EDGAR, B. A. 2020. Fitness trade-offs incurred by ovary-to-gut steroid signalling in Drosophila. *Nature,* 584**,** 415-419.

ARANDA, A. & PASCUAL, A. 2001. Nuclear hormone receptors and gene expression. *Physiol Rev,* 81**,** 1269-304.

BAKER, J. M., AL-NAKKASH, L. & HERBST-KRALOVETZ, M. M. 2017. Estrogen-gut microbiome axis: Physiological and clinical implications. *Maturitas,* 103**,** 45-53.

BLACKIE, L., GASPAR, P., MOSLEH, S., LUSHCHAK, O., KONG, L., JIN, Y., ZIELINSKA, A. P., CAO, B., MINEO, A., SILVA, B., AMEKU, T., LIM, S. E., MAO, Y., PRIETO-GODINO, L., SCHOBORG, T., VARELA, M., MAHADEVAN, L. & MIGUEL-ALIAGA, I. 2024. The sex of organ geometry. *Nature,* 630**,** 392-400.

BOULAN, L., MILAN, M. & LEOPOLD, P. 2015. The Systemic Control of Growth. *Cold Spring Harb Perspect Biol,* 7.

BROWN, J. B., BOLEY, N., EISMAN, R., MAY, G. E., STOIBER, M. H., DUFF, M. O., BOOTH, B. W., WEN, J., PARK, S., SUZUKI, A. M., WAN, K. H., YU, C., ZHANG, D., CARLSON, J. W., CHERBAS, L., EADS, B. D., MILLER, D., MOCKAITIS, K., ROBERTS, J., DAVIS, C. A., FRISE, E., HAMMONDS, A. S., OLSON, S., SHENKER, S., STURGILL, D., SAMSONOVA, A. A., WEISZMANN, R., ROBINSON, G., HERNANDEZ, J., ANDREWS, J., BICKEL, P. J., CARNINCI, P., CHERBAS, P., GINGERAS, T. R., HOSKINS, R. A., KAUFMAN, T. C., LAI, E. C., OLIVER, B., PERRIMON, N., GRAVELEY, B. R. & CELNIKER, S. E. 2014. Diversity and dynamics of the Drosophila transcriptome. *Nature,* 512**,** 393-9.

CHUNG, H., SZTAL, T., PASRICHA, S., SRIDHAR, M., BATTERHAM, P. & DABORN, P. J. 2009. Characterization of Drosophila melanogaster cytochrome P450 genes. *Proc Natl Acad Sci U S A,* 106**,** 5731-6.

COLOMBANI, J., RAISIN, S., PANTALACCI, S., RADIMERSKI, T., MONTAGNE, J. & LEOPOLD, P. 2003. A nutrient sensor mechanism controls Drosophila growth. *Cell,* 114**,** 739-49.

ERKOSAR, B., STORELLI, G., MITCHELL, M., BOZONNET, L., BOZONNET, N. & LEULIER, F. 2015. Pathogen Virulence Impedes Mutualist-Mediated Enhancement of Host Juvenile Growth via Inhibition of Protein Digestion. *Cell Host Microbe,* 18**,** 445-55.

ERVIN, S. M., LI, H., LIM, L., ROBERTS, L. R., LIANG, X., MANI, S. & REDINBO, M. R. 2019. Gut microbial beta-glucuronidases reactivate estrogens as components of the estrobolome that reactivate estrogens. *J Biol Chem,* 294**,** 18586-18599.

GEMINARD, C., RULIFSON, E. J. & LEOPOLD, P. 2009. Remote control of insulin secretion by fat cells in Drosophila. *Cell Metab,* 10**,** 199-207.

GRENIER, T., CONSUEGRA, J., FERRARINI, M. G., AKHERRAZ, H., BAI, L., DUSABYINEMA, Y., RAHIOUI, I., DA SILVA, P., GILLET, B., HUGHES, S., RAMOS, C. I., MATOS, R. C. & LEULIER, F. 2023. Intestinal GCN2 controls Drosophila systemic growth in response to Lactiplantibacillus plantarum symbiotic cues encoded by r/tRNA operons. *Elife,* 12.

HU, S., DING, Q., ZHANG, W., KANG, M., MA, J. & ZHAO, L. 2023. Gut microbial beta-glucuronidase: a vital regulator in female estrogen metabolism. *Gut Microbes,* 15**,** 2236749.

HUXLEY, J. S. 1924. Constant Differential Growth-Ratios and their Significance. *Nature,* 114**,** 895-896.

MA, D., STORELLI, G., MITCHELL, M. & LEULIER, F. 2015. Studying host-microbiota mutualism in Drosophila: Harnessing the power of gnotobiotic flies. *Biomed J,* 38**,** 285-93.
MARTINEZ, E., GIVEL, F. & WAHLI, W. 1991. A common ancestor DNA motif for invertebrate and vertebrate hormone response elements. *EMBO J,* 10**,** 263-8.
MATOS, R. C., SCHWARZER, M., GERVAIS, H., COURTIN, P., JONCOUR, P., GILLET, B., MA, D., BULTEAU, A. L., MARTINO, M. E., HUGHES, S., CHAPOT-CHARTIER, M. P. & LEULIER, F. 2017. D-Alanylation of teichoic acids contributes to Lactobacillus plantarum-mediated Drosophila growth during chronic undernutrition. *Nat Microbiol,* 2**,** 1635-1647.
OBERDORSTER, E., CLAY, M. A., COTTAM, D. M., WILMOT, F. A., MCLACHLAN, J. A. & MILNER, M. J. 2001. Common phytochemicals are ecdysteroid agonists and antagonists: a possible evolutionary link between vertebrate and invertebrate steroid hormones. *J Steroid Biochem Mol Biol,* 77**,** 229-38.
OKAMOTO, N., VISWANATHA, R., BITTAR, R., LI, Z., HAGA-YAMANAKA, S., PERRIMON, N. & YAMANAKA, N. 2018. A Membrane Transporter Is Required for Steroid Hormone Uptake in Drosophila. *Dev Cell,* 47**,** 294-305 e7.
OKAMOTO, N. & YAMANAKA, N. 2020. Steroid Hormone Entry into the Brain Requires a Membrane Transporter in Drosophila. *Curr Biol,* 30**,** 359-366 e3.
PETRYK, A., WARREN, J. T., MARQUES, G., JARCHO, M. P., GILBERT, L. I., KAHLER, J., PARVY, J. P., LI, Y., DAUPHIN-VILLEMANT, C. & O'CONNOR, M. B. 2003. Shade is the Drosophila P450 enzyme that mediates the hydroxylation of ecdysone to the steroid insect molting hormone 20-hydroxyecdysone. *Proc Natl Acad Sci U S A,* 100**,** 13773-8.
PIGLIUCCI, M. 2001. *Phenotypic Plasticity: Beyond Nature and Nurture*, Johns Hopkins University Press.
SHIN, S. C., KIM, S. H., YOU, H., KIM, B., KIM, A. C., LEE, K. A., YOON, J. H., RYU, J. H. & LEE, W. J. 2011. Drosophila microbiome modulates host developmental and metabolic homeostasis via insulin signaling. *Science,* 334**,** 670-4.
SHINGLETON, A. W., DAS, J., VINICIUS, L. & STERN, D. L. 2005. The temporal requirements for insulin signaling during development in Drosophila. *PLoS Biol,* 3**,** e289.
STORELLI, G., DEFAYE, A., ERKOSAR, B., HOLS, P., ROYET, J. & LEULIER, F. 2011. Lactobacillus plantarum promotes Drosophila systemic growth by modulating hormonal signals through TOR-dependent nutrient sensing. *Cell Metab,* 14**,** 403-14.
STORELLI, G., STRIGINI, M., GRENIER, T., BOZONNET, L., SCHWARZER, M., DANIEL, C., MATOS, R. & LEULIER, F. 2018. Drosophila Perpetuates Nutritional Mutualism by Promoting the Fitness of Its Intestinal Symbiont Lactobacillus plantarum. *Cell Metab,* 27**,** 362-377 e8.
WING, K. D. 1988. RH 5849, a nonsteroidal ecdysone agonist: effects on a Drosophila cell line. *Science,* 241**,** 467-9.
YAMANAKA, N., MARQUES, G. & O'CONNOR, M. B. 2015. Vesicle-Mediated Steroid Hormone Secretion in Drosophila melanogaster. *Cell,* 163**,** 907-19.
ZIPPER, L., COROMINAS-MURTRA, B. & REIFF, T. 2025. Steroid hormone-induced wingless ligands tune female intestinal size in Drosophila. *Nat Commun,* 16**,** 436.
ZIPPER, L., JASSMANN, D., BURGMER, S., GORLICH, B. & REIFF, T. 2020. Ecdysone steroid hormone remote controls intestinal stem cell fate decisions via the PPARgamma-homolog Eip75B in Drosophila. *Elife,* 9.

Figure 1

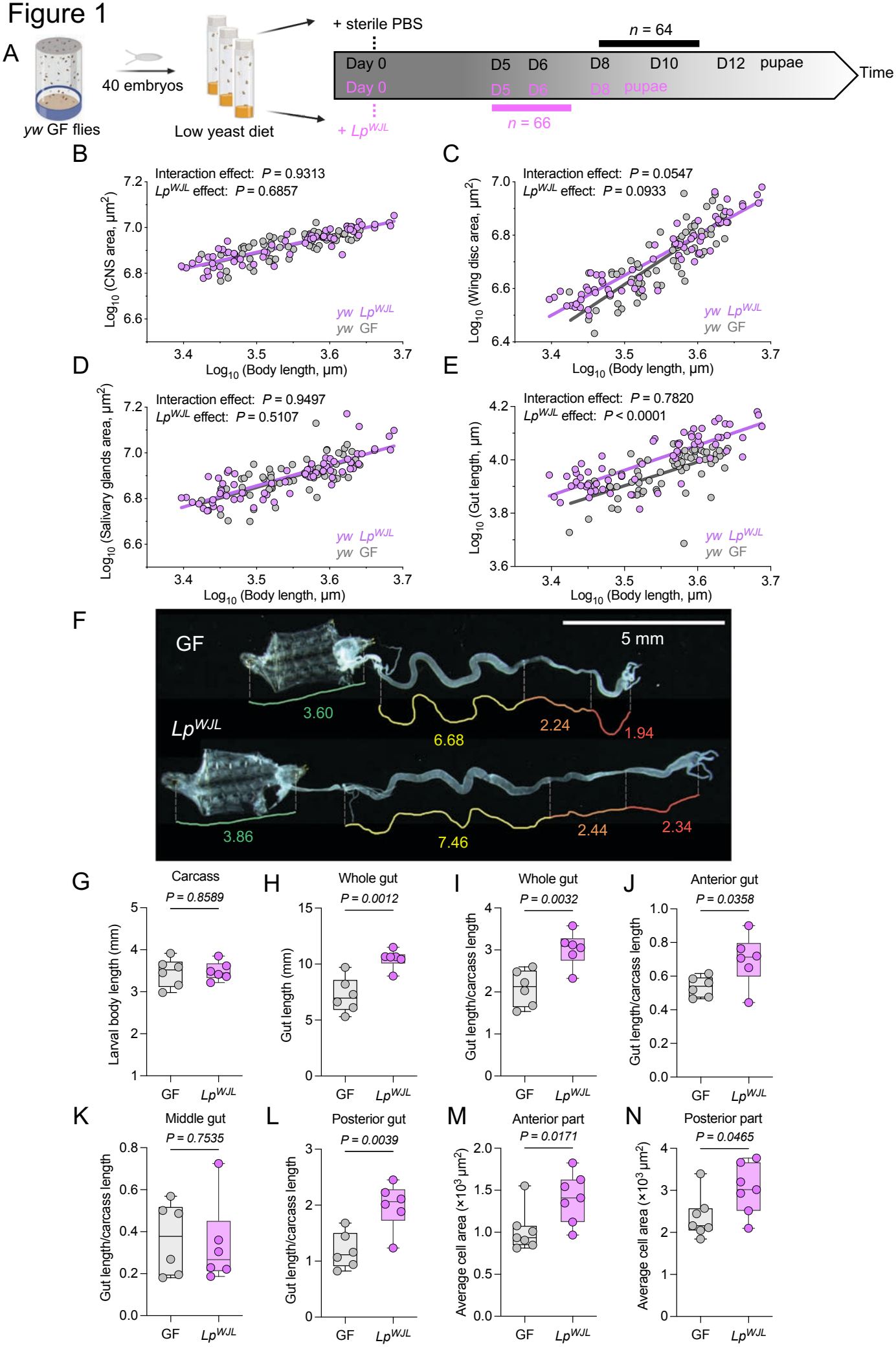
A
yw GF flies
40 embryos
Low yeast diet
+ sterile PBS
+ Lp^WJL
n = 64
n = 66
Day 0
D5
D6
D8
D10
D12
pupae
Time
B
Interaction effect: P = 0.9313
Lp^WJL effect: P = 0.6857
Log10 (CNS area, μm2)
Log10 (Body length, μm)
C
Interaction effect: P = 0.0547
Lp^WJL effect: P = 0.0933
Log10 (Wing disc area, μm2)
D
Interaction effect: P = 0.9497
Lp^WJL effect: P = 0.5107
Log10 (Salivary glands area, μm2)
E
Interaction effect: P = 0.7820
Lp^WJL effect: P < 0.0001
Log10 (Gut length, μm)
yw Lp^WJL
yw GF
F
GF
Lp^WJL
5 mm
3.60
6.68
2.24
1.94
3.86
7.46
2.44
2.34
G
Carcass
P = 0.8589
Larval body length (mm)
H
Whole gut
P = 0.0012
Gut length (mm)
I
Whole gut
P = 0.0032
Gut length/carcass length
J
Anterior gut
P = 0.0358
K
Middle gut
P = 0.7535
L
Posterior gut
P = 0.0039
M
Anterior part
P = 0.0171
Average cell area (×10³ μm²)
N
Posterior part
P = 0.0465
GF
Lp^WJL

Figure 2

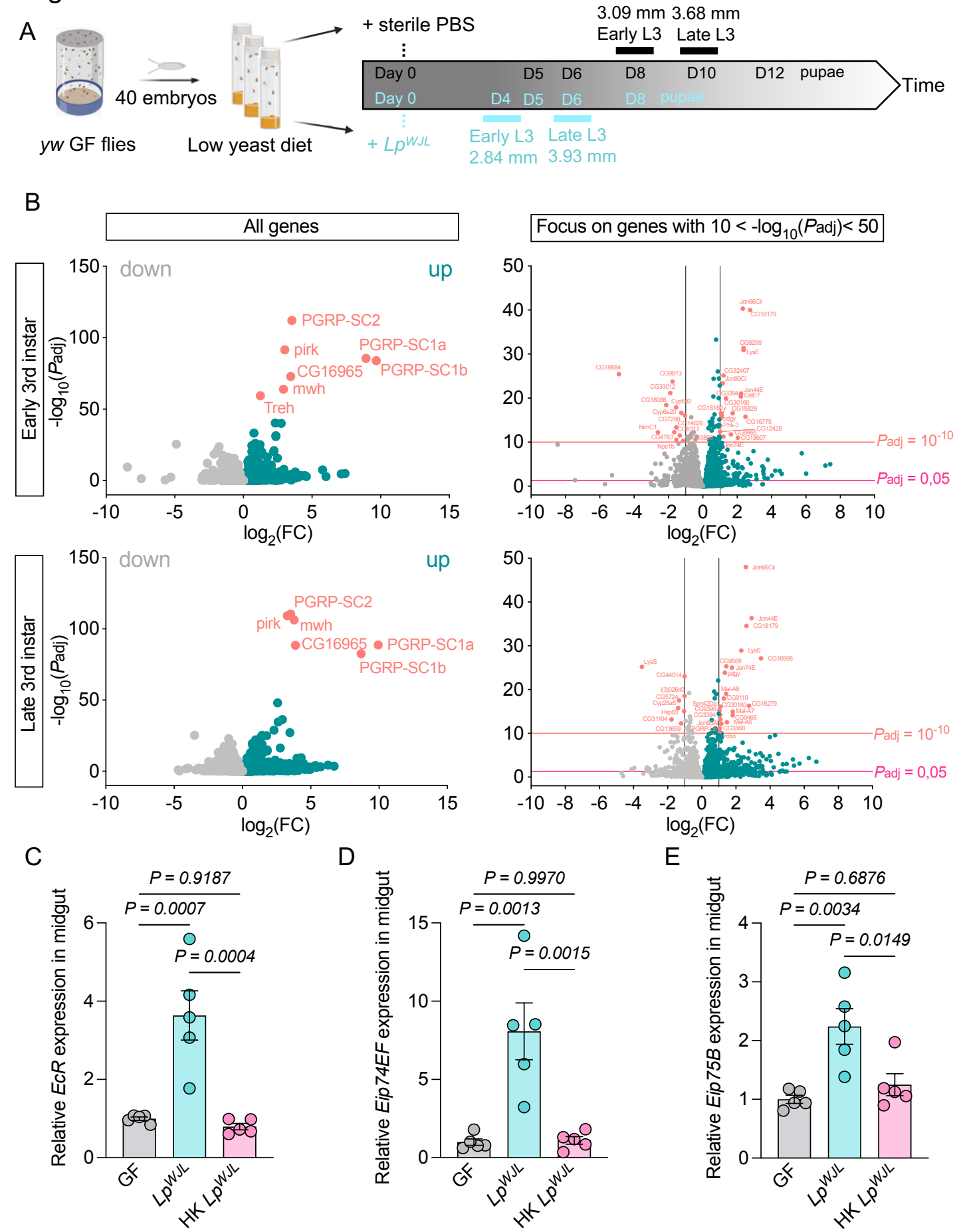
A
40 embryos
yw GF flies
Low yeast diet
+ sterile PBS
+ LpWJL
3.09 mm
Early L3
3.68 mm
Late L3
Day 0
D5
D6
D8
D10
D12
pupae
Time
Day 0
D4
D5
D6
D8
pupae
Early L3
2.84 mm
Late L3
3.93 mm
B
All genes
Focus on genes with 10 < -log10(Padj)< 50
Early 3rd instar
Late 3rd instar
down
up
PGRP-SC2
pirk
PGRP-SC1a
CG16965
PGRP-SC1b
mwh
Treh
-log10(Padj)
log2(FC)
Padj = 10-10
Padj = 0,05
C
D
E
P = 0.9187
P = 0.0007
P = 0.0004
P = 0.9970
P = 0.0013
P = 0.0015
P = 0.6876
P = 0.0034
P = 0.0149
Relative EcR expression in midgut
Relative Eip74EF expression in midgut
Relative Eip75B expression in midgut
GF
LpWJL
HK LpWJL

Figure 3

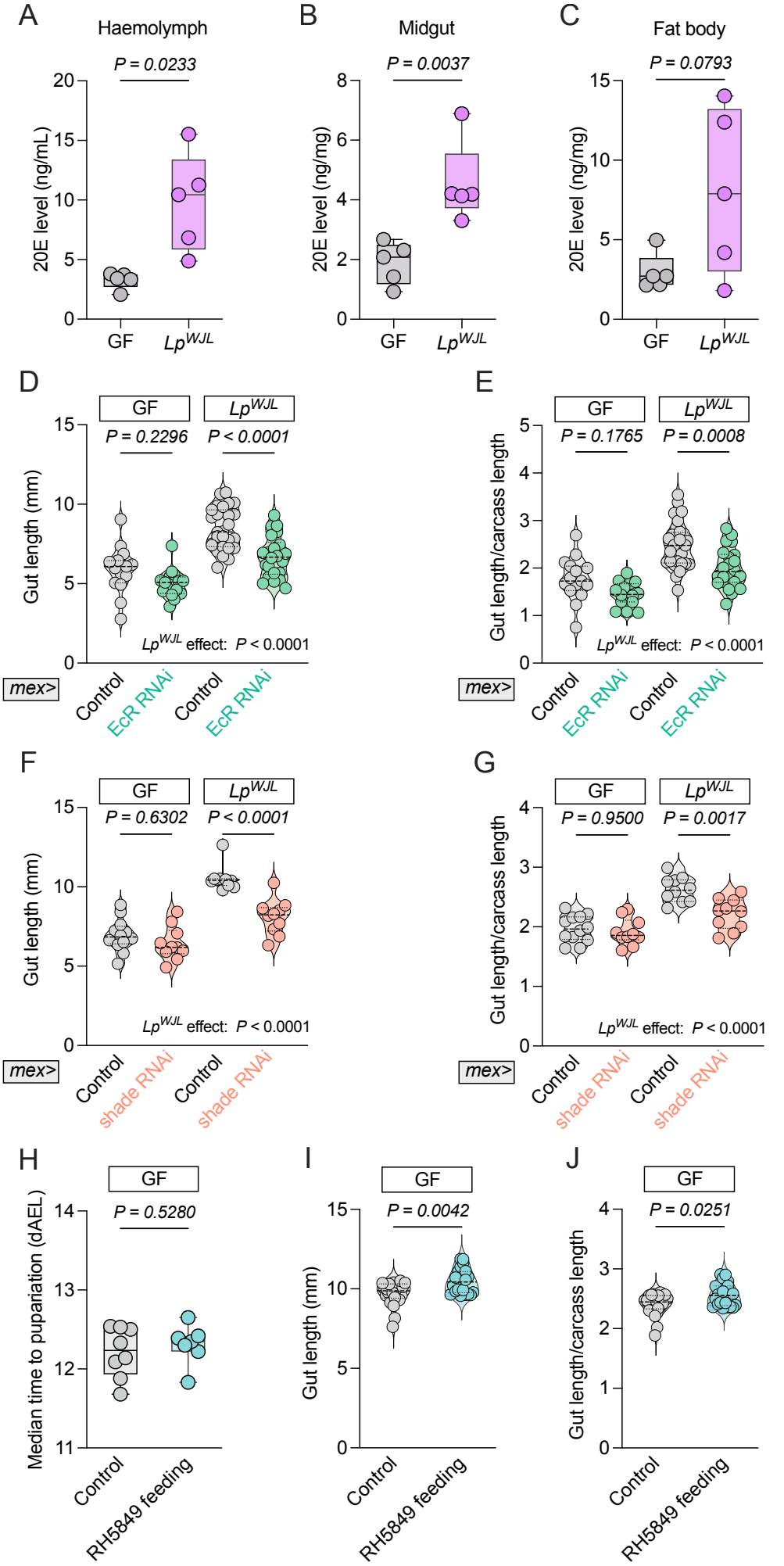
A
Haemolymph
P = 0.0233
20E level (ng/mL)
GF
LpWJL
B
Midgut
P = 0.0037
20E level (ng/mg)
C
Fat body
P = 0.0793
D
GF
LpWJL
P = 0.2296
P < 0.0001
Gut length (mm)
LpWJL effect: P < 0.0001
mex>
Control
EcR RNAi
E
P = 0.1765
P = 0.0008
Gut length/carcass length
F
P = 0.6302
shade RNAi
G
P = 0.9500
H
Median time to pupariation (dAEL)
RH5849 feeding
I
P = 0.0042
J
P = 0.0251

Figure 4

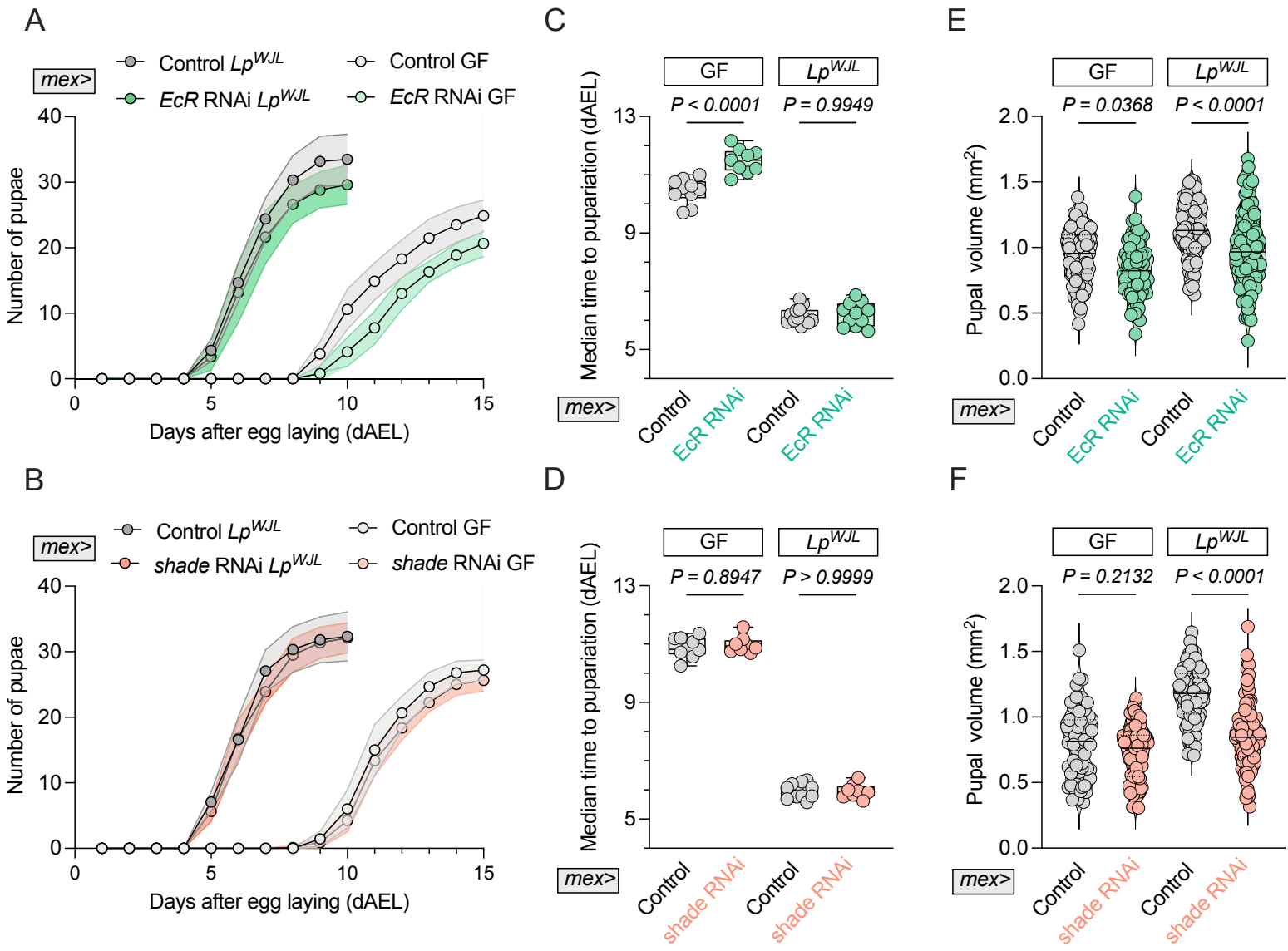
A
mex>
Control Lp^{WJL}
EcR RNAi Lp^{WJL}
Control GF
EcR RNAi GF
Number of pupae
Days after egg laying (dAEL)
B
mex>
Control Lp^{WJL}
shade RNAi Lp^{WJL}
Control GF
shade RNAi GF
Number of pupae
Days after egg laying (dAEL)
C
GF
Lp^{WJL}
P < 0.0001
P = 0.9949
Median time to pupariation (dAEL)
mex>
Control
EcR RNAi
Control
EcR RNAi
D
GF
Lp^{WJL}
P = 0.8947
P > 0.9999
Median time to pupariation (dAEL)
mex>
Control
shade RNAi
Control
shade RNAi
E
GF
Lp^{WJL}
P = 0.0368
P < 0.0001
Pupal volume (mm^2)
mex>
Control
EcR RNAi
Control
EcR RNAi
F
GF
Lp^{WJL}
P = 0.2132
P < 0.0001
Pupal volume (mm^2)
mex>
Control
shade RNAi
Control
shade RNAi

Figure S1

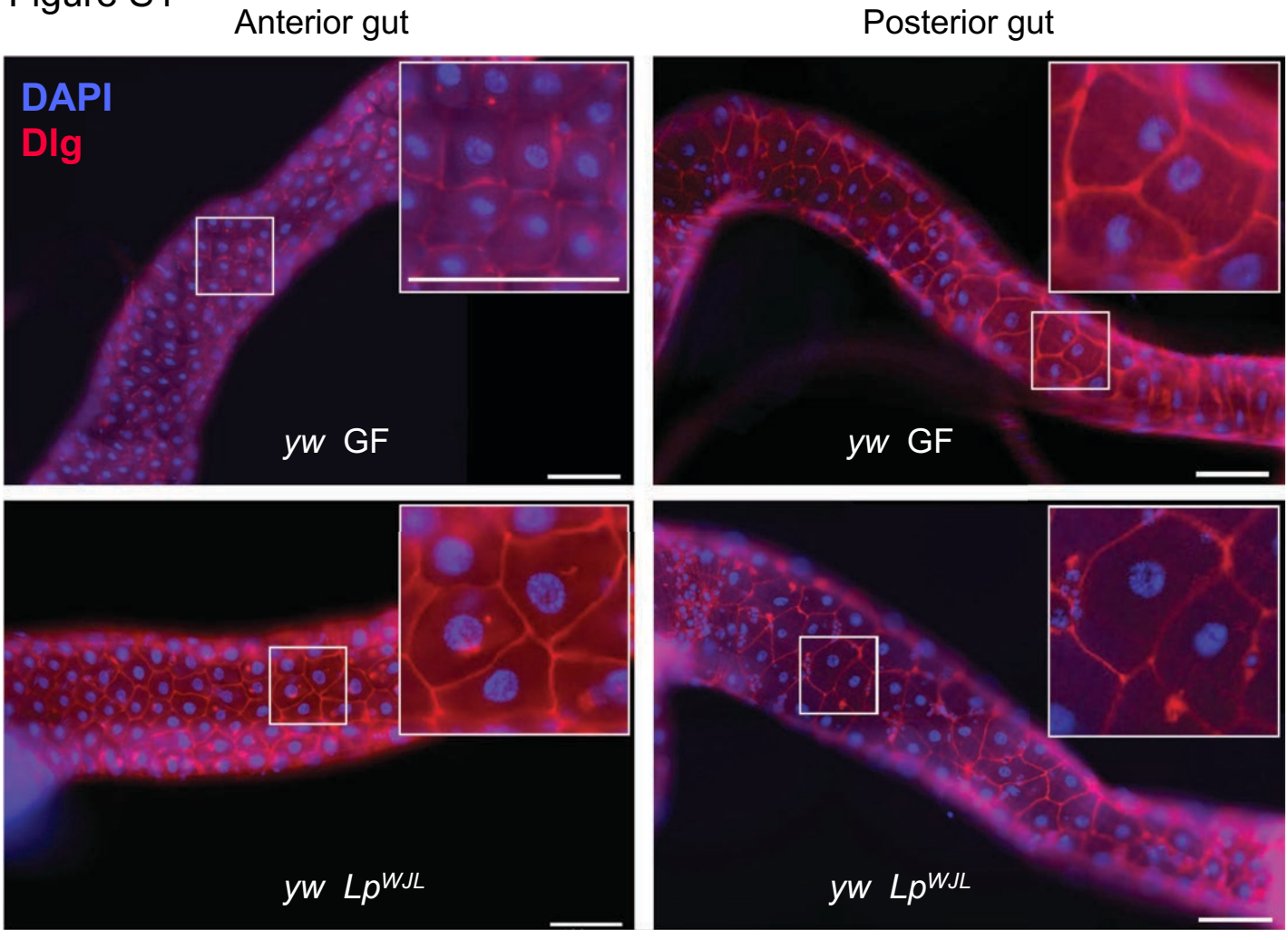
Anterior gut
Posterior gut
DAPI
Dlg
yw GF
yw GF
yw Lp^WJL
yw Lp^WJL

Figure S2

A

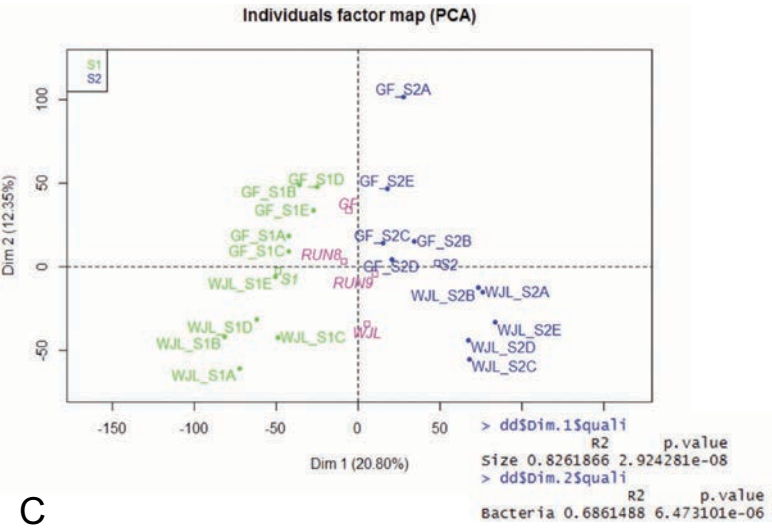

B

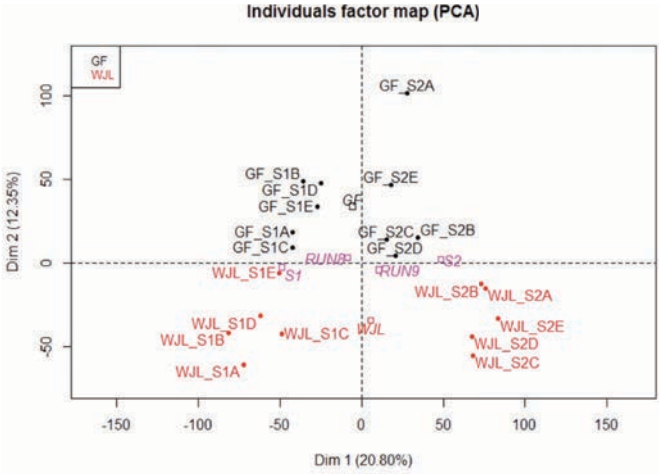

C

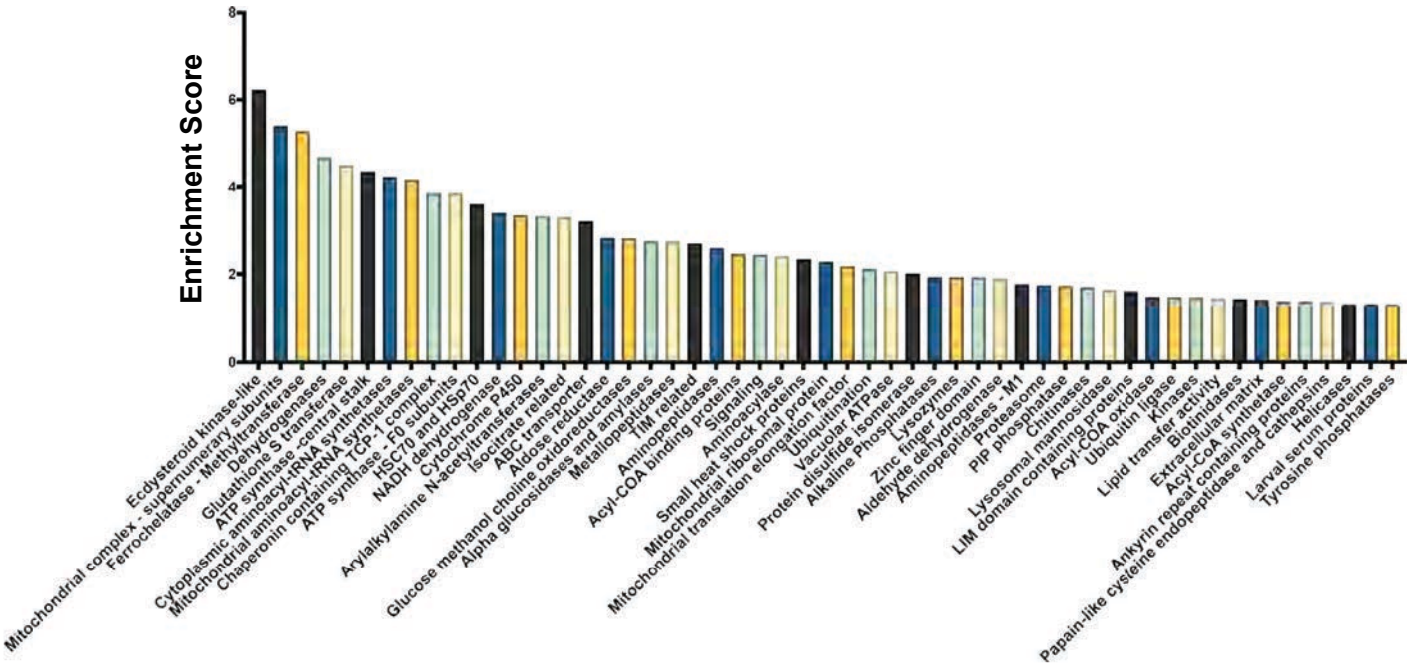

D

Flybase reference	Gene name
FBgn0039311	CG10513 gene product from transcript CG10513-RB(CG10513)
FBgn0052195	CG32195 gene product from transcript CG32195-RA(CG32195)
FBgn0039310	CG11878 gene product from transcript CG11878-RA(CG11878)
FBgn0031801	CG9498 gene product from transcript CG9498-RA(CG9498)
FBgn0051974	CG31974 gene product from transcript CG31974-RB(CG31974)
FBgn0030060	CG2004 gene product from transcript CG2004-RG(CG2004)
FBgn0051102	CG31102 gene product from transcript CG31102-RA(CG31102)
FBgn0039309	CG11891 gene product from transcript CG11891-RD(CG11891)
FBgn0031320	CG5126 gene product from transcript CG5126-RA(CG5126)
FBgn0042110	CG18765 gene product from transcript CG18765-RB(CG18765)
FBgn0028424	Juvenile hormone-inducible protein 26(Jhl-26)
FBgn0051975	CG31975 gene product from transcript CG31975-RC(CG31975)
FBgn0045761	CG10618 gene product from transcript CG10618-RE(CHKov1)
FBgn0039326	CG10562 gene product from transcript CG10562-RA(CG10562)
FBgn0039325	CG10560 gene product from transcript CG10560-RA(CG10560)
FBgn0053510	CG33510 gene product from transcript CG33510-RB(CG33510)
FBgn0039324	CG10553 gene product from transcript CG10553-RA(CG10553)
FBgn0051087	CG31087 gene product from transcript CG31087-RA(CG31087)
FBgn0039321	CG10550 gene product from transcript CG10550-RD(CG10550)
FBgn0039319	CG13659 gene product from transcript CG13659-RA(CG13659)
FBgn0051097	CG31097 gene product from transcript CG31097-RB(CG31097)
FBgn0053301	CG33301 gene product from transcript CG33301-RB(CG33301)
FBgn0051098	CG31098 gene product from transcript CG31098-RA(CG31098)
FBgn0039316	CG11893 gene product from transcript CG11893-RA(CG11893)
FBgn0039308	CG11889 gene product from transcript CG11889-RA(CG11889)
FBgn0039315	CG13658 gene product from transcript CG13658-RB(CG13658)
FBgn0037936	CG6908 gene product from transcript CG6908-RA(CG6908)
FBgn0051104	CG31104 gene product from transcript CG31104-RA(CG31104)
FBgn0037934	CG6830 gene product from transcript CG6830-RA(CG6830)
FBgn0039312	CG10514 gene product from transcript CG10514-RA(CG10514)

Figure S3

Response to Ecdysone

TOR signaling
negative regulation of TOR signaling
positive regulation of TOR signaling
negative regulation of insulin receptor signaling pathway

Lipid metabolism
regulation of lipid storage
triglycerides homeostasis
lipid metabolic process
fatty acid beta-oxidation
fatty acid biosynthetic process
sphingolipid metabolic process
phospholipid biosynthetic process
regulation of lipid meatbolic process
cholesterol homeostasis
long-chain fatty-acid biosynthetic process

Autophagy and response to cellular stress
cellular response to DNA damage stimulus
cellular response to oxidative stress
response to ER stress
salivary gland cell autophagic cell death
cellular response to starvation
negative regulation of autophagy
regulation of autophagy
autophagy
autophagic cell death
detoxification of arsenic-containing substance
cellular response to amino-acid starvation
phagocytosis, engulfment

Oxido - reduction
oxidation-reduction process
glutathione metabolic process
glutathione biosynthetic process

Transcription/Translation
chaperon-mediated protein folding
nitrogen compound metabolic process
SRP-dependent cotranslational protein targeting to memebrane
signal peptide processing
protein folding
translational initiation
cellular response to unfolded protein
protein complex assembly
formation of translation preinitiation complex
maturation o SSU-rRNA from tricistronic rRNA transcripts
nuclear-transcribed mRNA poly(A) tail shortening
positive regulation of transcription of transcription from RNA polymerase II promoter
regulation of chromatin silencing
regulation of alternativemRNA splicing via spliceosome

Others
cold acclimatation
determination of adult lifespan
sperm individualization
sensory perception of pain
flavonoid biosynthetic process
flavonoid glucuronidation
behavioral response to ethanol sleep

Size 1 - Early 3rd instar

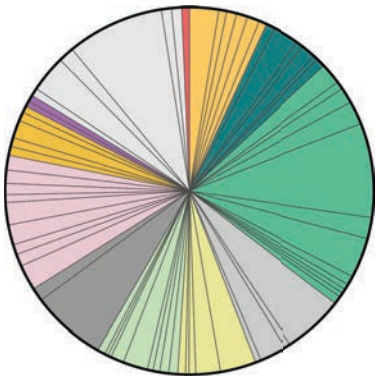

Size 2 - Late 3rd instar

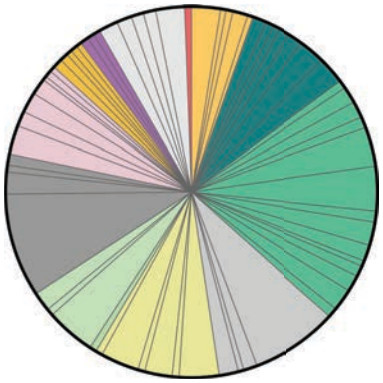

Metabolism
metabolic process
carbohydrate metabolic process
glucose metabolic process
GDP-mannose biosynthetic process
insecticide catabolic process
glucose homeostasis
isoprenoid biosynthetic process
regulation of glucose metabolic process
response to methotrexate

Mitochondria
translation
electron transport
proton transport
organization
ATP synthesis coupled proton transport
translational elongation
respiratory chain complex IV assembly
organization
ubiquinone biosynthetic process

Immunity
cell wall macromolecule catabolic process
defense response to Gram-neg bacterium
negative regulation of innate immune response
negative regulation of peptidoglycan recognition protein signaling pathway
peptidoglycan catabolic process
antimicrobial humoral response
cell wall macromolecule catabolic process
negative regulation of growth of symbiont in host
negative regulation of innate immune response
defense response to Gram- bacterium
immune response

Development and cell growth
chaeta development
cytolysis
cell morphogenesis
chitin metabolic process
neurogenesis
wing disc development
lateral inhibition
neuron cellular homeostasis
Arp2/3 actin nucleation
negative regulation of actin filament polymerization
regulation of lamellipodium assembly
centriole replication
negative regulation of cell proliferation
wing disc dorsal/ventral pattern formation
regulation of hemocyte proliferation
dendrite morphogenesis
positive regulation at NMJcell adhesion
heart developmentpostive regultation of cell size
axonogenesis
regulation of cell cycle
regulation of growth

Transport and signaling
transport
regulation of intracellular pH
transmembrane transport
dephosphorylation
molybdoterin cofactor biosynthetic process
aminoacid transmembrane transport
chloride transmembrane transport

Figure S4

A

		Size 1 WJL effect						Size 2 WJL effect					
Gene ID	Gene name	Mean GF	Mean Lp WJL	FC	Reg	p value	p adj	Mean GF	Mean Lp WJL	FC	Reg	p value	p adj
FBgn0000546	EcR	219,433481	218,92924	-1,0023032	0	0,95305101	0,9799303	282,422619	426,943507	1,51171853	up	3,75E-09	3,19E-07
FBgn0003964	usp	310,498518	295,311489	-1,0514272	0	0,48461153	0,705275	382,78872	407,42331	1,06435558	0	0,37446915	0,63676016
FBgn0035542	DOR	597,670613	858,425821	1,43628581	up	0,00035996	0,00417176	857,095662	1473,39823	1,71905925	up	4,55E-07	2,14E-05
FBgn0030597	Eo	12,2207685	18,7737175	1,53621415	0	0,08730855	0,25170521	41,4890487	78,5917788	1,89427768	up	0,00239656	0,02113901
FBgn0023518	trr	266,890387	216,611317	-1,2321165	down	0,00283641	0,02126736	267,94401	255,281174	-1,0496035	0	0,31531492	0,58295418
FBgn0000139	ash2	349,319242	212,208716	-1,6461117	down	4,47E-14	6,18E-12	359,697295	335,075656	-1,0734808	0	0,18732613	0,43421894
FBgn0000568	Eip75B	540,632815	433,650906	-1,2467005	down	0,00512957	0,03328649	566,182956	850,193166	1,50162268	up	1,74E-07	9,23E-06
FBgn0004910	Eip63F-1	821,250944	1066,86965	1,29907875	up	0,0082984	0,04755149	990,871452	1243,3331	1,25478749	0	0,02065754	0,10378637
FBgn0000567	Eip74EF	25,7946648	28,8884835	1,11994026	0	0,5760315	0,77103956	40,4795348	109,233679	2,69849145	up	4,62E-08	2,97E-06
FBgn0000565	Eip71CD	127,128855	273,392206	2,15051261	up	0,00011906	0,0016781	104,388567	143,305187	1,37280538	0	0,12945874	0,34511107
FBgn0000568	Eip75B	540,632815	433,650906	-1,2467005	down	0,00512957	0,03328649	566,182956	850,193166	1,50162268	up	1,74E-07	9,23E-06
FBgn0004910	Eip63F-1	821,250944	1066,86965	1,29907875	up	0,0082984	0,04755149	990,871452	1243,3331	1,25478749	0	0,02065754	0,10378637
FBgn0005640	Eip63E	236,432402	274,823954	1,16237856	up	0,00821473	0,04721813	240,608631	272,187693	1,13124659	0	0,04186751	0,16791637
FBgn0000566	Eip55E	1291,9916	1330,47884	1,02978908	0	0,58679995	0,77858827	1030,35025	771,979457	-1,3346861	down	2,83E-06	9,85E-05
FBgn0001257	ImpL2	1866,23864	1004,6364	-1,8576259	down	7,63E-08	3,02E-06	1710,61713	1265,0659	-1,3521961	down	0,00754404	0,04992947
FBgn0001258	ImpL3	1122,96709	474,275444	-2,367753	down	1,09E-06	3,13E-05	789,624376	510,464932	-1,5468729	0	0,01337085	0,07551596
FBgn0001254	ImpE2	6,69934854	3,88152121	-1,7259595	0	0,20766781	0,43210368	7,0697174	1,10675487	-6,3877897	down	0,00272519	0,02326161
FBgn0015240	Hr96	1032,34666	629,553426	-1,6398079	down	9,87E-09	5,22E-07	654,903108	539,857647	-1,2131033	0	0,03113611	0,13719523
FBgn0283451	br	182,273732	267,069166	1,46520929	up	0,00011848	0,00167442	317,513885	618,914076	1,94925043	up	1,85E-12	2,66E-10
FBgn0024509	Sec13	497,188729	628,754046	1,26461846	up	0,0034175	0,02468493	504,079847	511,71935	1,01515534	0	0,86730391	0,94761162
FBgn0010051	Itp-r83A	674,91903	568,236373	-1,1877435	down	0,00381744	0,02675966	610,211711	605,533767	-1,0077253	0	0,98460585	0,99477529
FBgn0002562	Lsp1alpha	679,154586	1966,55427	2,89559153	up	0,00734666	0,0436085	3334,87558	5204,61782	1,56066327	0	0,11880745	0,32792734
FBgn0002563	Lsp1beta	1038,45041	6062,88442	5,83839574	up	0,00012663	0,00176328	19183,7128	42080,1389	2,19353466	0	0,06053795	0,21393868
FBgn0002564	Lsp1gamma	1830,01782	7387,61568	4,03690916	up	0,00039202	0,00447059	12981,8725	36181,6369	2,78708922	up	0,00716513	0,04852395
FBgn0002565	Lsp2	1,2765747	179,707651	140,773313	up	6,82E-07	2,11E-05	818,395656	3185,7447	3,89267059	0	0,23579137	0,49495948
FBgn0000640	Fbp2	2,52328811	30,3649324	12,0338745	up	0,00131716	0,0116272	60,9203564	328,081574	5,38541783	up	0,00493484	0,03665344
FBgn0050277	Oatp58Da	10,4070405	6,74985326	-1,5418173	0	0,3914044	0,6276025	5,69536877	31,725292	5,57036661	up	0,00188523	0,01754645
FBgn0034716	Oatp58Dc	34,2874337	21,3874765	-1,6031547	0	0,4395995	0,669742	12,0883163	113,337427	9,37578271	up	0,00019656	0,0031729
FBgn0036732	Oatp74D	351,616714	407,844158	1,15991118	0	0,1145276	0,2978627	741,732234	1155,48274	1,55781653	up	1,43E-06	5,57E-05

B

		Size1 WJL vs GF						Size2 WJL vs GF					
Gene_ID	gene_name	Mean_GF	Mean_WJL	FC	Reg	pvalue	padj	Mean_GF	Mean_WJL	FC	Reg	pvalue	padj
FBgn0283499	InR	166,531232	165,658455	-1,0052685	0	0,9869939	0,9941872	144,433829	154,257757	1,0680168	0	0,57768002	0,79057806
FBgn0036046	Ilp2	4,67108996	2,88012313	-1,6218369	0	0,7985765	NA	5,50394323	0	-Inf	0	0,34243618	0,60704275
FBgn0036690	Ilp8	0,52692036	0	-Inf	0	0,7361203	NA	0	0	NA	0	0,94237624	NA
FBgn0044046	Ilp7	0	0,24471534	Inf	0	0,8453244	NA	0,18386189	0,25814914	1,40403833	0	0,95950707	NA
FBgn0044047	Ilp6	7,57638431	10,6083348	1,40018435	0	0,333673	0,5708059	10,1358068	16,1888851	1,59719749	0	0,07288603	0,24213018
FBgn0044048	Ilp5	1,16904986	0,77118533	-1,515913	0	0,9003219	NA	3,12274648	0	-Inf	0	0,47358582	NA
FBgn0044049	Ilp4	0	0,27533127	Inf	0	0,8453226	NA	0	0	NA	0	0,93737123	NA
FBgn0044050	Ilp3	409,703235	355,721331	-1,1517534	0	0,03836448	0,1442367	635,428987	633,106929	-1,0036677	0	0,97386427	0,99016114
FBgn0044051	Ilp1	0	0	NA	0	NA	NA	0	0	NA	0	NA	NA
FBgn0024248	chico	672,0762	637,734326	-1,0538498	0	0,45187916	0,68005867	657,837915	760,164236	1,15554944	0	0,06141686	0,21595245
FBgn0015279	Pi3K92E	681,265482	678,936127	-1,0034309	0	0,97272189	0,9878577	632,352665	682,47214	1,07925874	0	0,22571372	0,48303032
FBgn0010379	Akt1	561,767144	580,674043	1,03365611	0	0,4975727	0,71451319	508,889715	610,074887	1,19883517	up	0,00113146	0,01222976
FBgn0026317	Tsc1	300,611419	294,310867	-1,0214078	0	0,78228653	0,89808744	286,83912	273,552163	-1,0485719	0	0,58682329	0,7970897
FBgn0038197	foxo	265,188309	255,323223	-1,0386376	0	0,7012076	0,8515592	254,886738	350,682197	1,3758354	up	0,00013868	0,00236334
FBgn0021796	Tor	311,383452	306,592859	-1,0156253	0	0,84053743	0,92676084	316,704471	301,432361	-1,0506651	0	0,37962448	0,6414729
FBgn0261560	Thor	5835,75163	5255,12021	-1,1104887	0	0,4900612	0,7095008	3900,0697	6031,69555	1,54656096	0	0,01816579	0,09398427
FBgn0283472	S6k	1848,47355	1745,83625	-1,0587898	0	0,3256426	0,5624791	1857,86202	2144,51808	1,15429352	0	0,01465934	0,0806511
FBgn0261456	hpo	116,576008	112,009577	-1,0407682	0	0,6830984	0,8413323	129,929356	128,692676	-1,0096096	0	0,88882777	0,95556082
FBgn0011739	wts	218,171621	190,539399	-1,145021	0	0,05155874	0,17578569	224,651347	243,085191	1,08205535	0	0,31374302	0,58103638
FBgn0034970	yki	750,024913	682,933139	-1,0982406	0	0,2585943	0,4919029	916,172621	1086,07315	1,18544598	0	0,06235775	0,21777348
FBgn0262656	dmyc	565,517341	588,724664	1,04103733	0	0,7333652	0,8698555	428,947917	406,421228	-1,0554269	0	0,72789145	0,88132618
FBgn0003900	twi	1,78131278	1,22106771	-1,4588157	0	0,48408518	NA	2,33782819	0,78872873	-2,964046	0	0,17597629	NA
FBgn0003731	Egfr	278,524515	218,136306	-1,276837	down	0,00031849	0,00379071	299,551953	263,152053	-1,1383227	0	0,0530522	0,19621568
FBgn0004638	drk	755,050517	834,435096	1,1051381	0	0,23554268	0,46525709	733,488332	693,148271	-1,0581983	0	0,52708711	0,75700575
FBgn0003204	ras	364,834055	308,758049	-1,181618	down	0,00836278	0,04782849	294,64951	271,245911	-1,0862818	0	0,34025825	0,60540944
FBgn0004644	hh	69,4534627	66,1851854	-1,0493808	0	0,72436801	0,8643876	52,1908383	51,4897399	-1,0136163	0	0,89176439	0,95712522
FBgn0003444	smo	88,8568883	87,2220978	-1,0187428	0	0,99326965	0,99688506	91,7506121	80,8758842	-1,1344619	0	0,3203162	0,58847398
FBgn0003892	ptc	73,1212362	56,7828269	-1,287735	0	0,05654832	0,18694661	78,149471	58,8602165	-1,3277129	0	0,03514094	0,14887341
FBgn0010382	CycE	49,4224455	63,1154982	1,27706142	0	0,04372728	0,15755431	41,4200553	30,5882944	-1,3541146	0	0,0519115	0,19322614

Figure S5

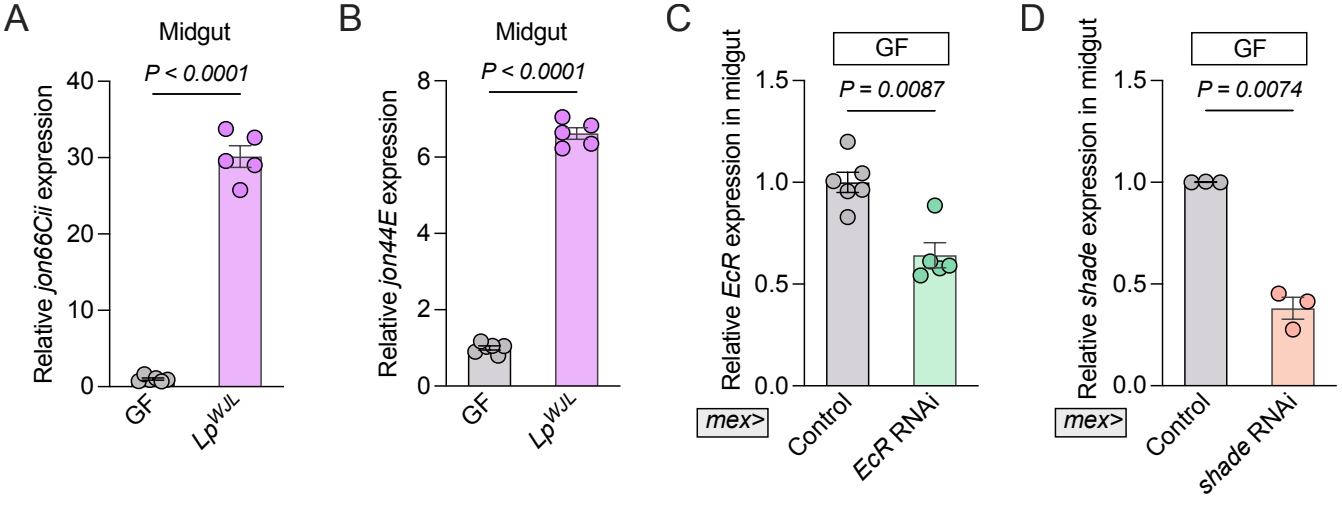
A
Midgut
P < 0.0001
Relative jon66Cii expression
40
30
20
10
0
GF
LpWJL
B
Midgut
P < 0.0001
Relative jon44E expression
8
6
4
2
0
GF
LpWJL
C
GF
P = 0.0087
Relative EcR expression in midgut
1.5
1.0
0.5
0.0
mex>
Control
EcR RNAi
D
GF
P = 0.0074
Relative shade expression in midgut
1.5
1.0
0.5
0.0
mex>
Control
shade RNAi

Figure S6

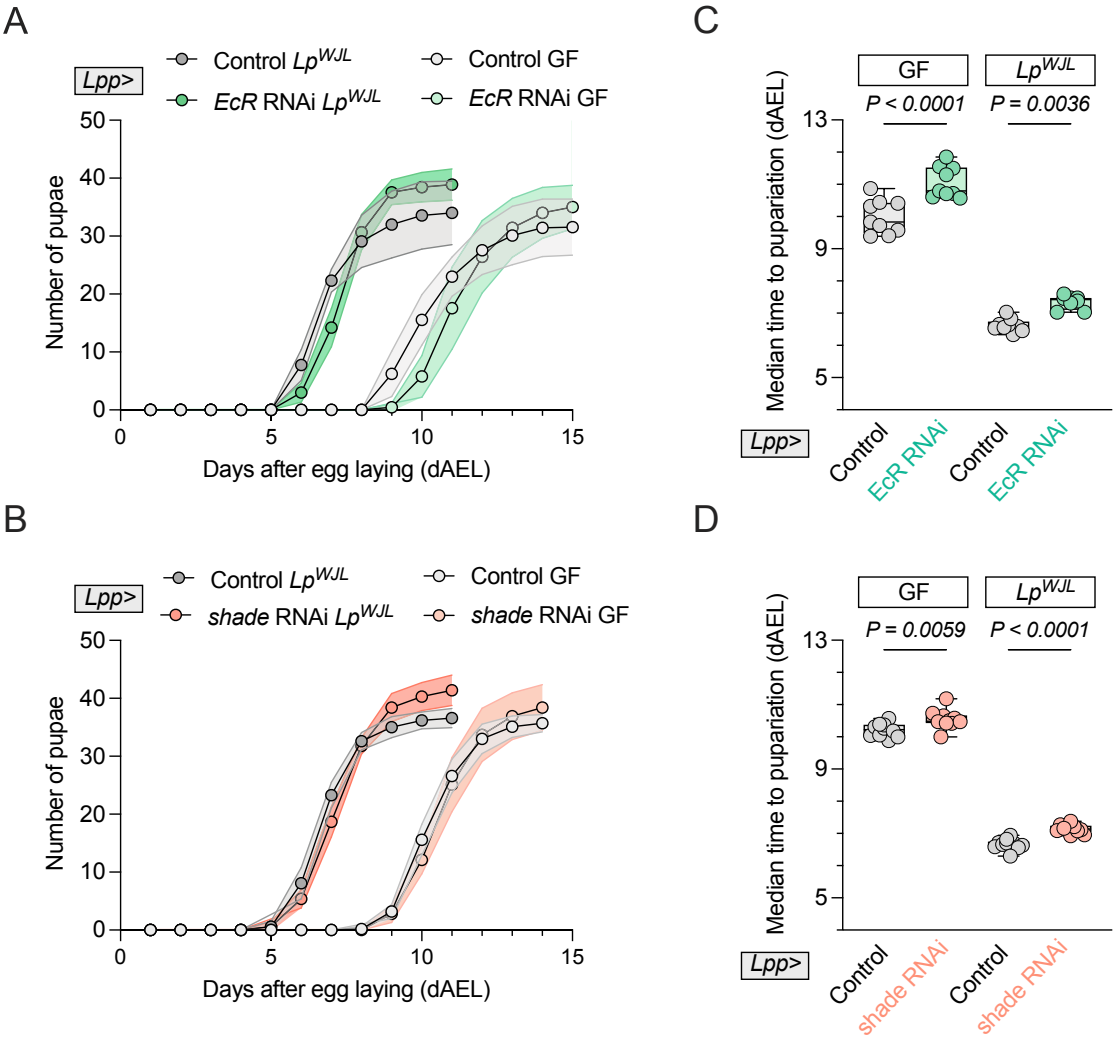
A
Lpp>
Control Lp^{WJL}
EcR RNAi Lp^{WJL}
Control GF
EcR RNAi GF
Number of pupae
Days after egg laying (dAEL)
B
Lpp>
Control Lp^{WJL}
shade RNAi Lp^{WJL}
Control GF
shade RNAi GF
Number of pupae
Days after egg laying (dAEL)
C
GF
Lp^{WJL}
P < 0.0001
P = 0.0036
Median time to pupariation (dAEL)
Lpp>
Control
EcR RNAi
Control
EcR RNAi
D
GF
Lp^{WJL}
P = 0.0059
P < 0.0001
Median time to pupariation (dAEL)
Lpp>
Control
shade RNAi
Control
shade RNAi